A Letters Journal Exploring the Frontiers of Physics

December 2011

EPL, **96** (2011) 59003
doi: 10.1209/0295-5075/96/59003

www.epljournal.org

Ultrafast ultrasonic imaging of dynamic sliding friction in soft solids: The slow slip and the super-shear regimes

S. Latour[1(a)], T. Gallot[1,2], S. Catheline[1], C. Voisin[1], F. Renard[1,3], E. Larose[1] and M. Campillo[1]

[1] *Institut des Sciences de la Terre, Université Joseph Fourier Grenoble I and CNRS - BP53, 38041 Grenoble, France, EU*
[2] *École Normale Supérieure de Lyon - 46 allée d'Italie, Lyon, France, EU*[(b)]
[3] *Physics of Geological Processes, University of Oslo - box 1047, 0316 Blindern, Norway*

received 27 July 2011; accepted in final form 17 October 2011
published online 24 November 2011

PACS 91.55.Fg – Dynamics and mechanics of faulting
PACS 62.20.Qp – Friction, tribology, and hardness

Abstract – Ultrafast ultrasonic speckle interferometry, an imaging technique derived from elastography, is used to follow the dynamic of the interface failure in a friction experiment. Experimental results that characterise two slipping regimes are presented: a slow slip regime associated with depinning events at the interface and a supershear rupture regime associated with the emission of Mach waves fronts. These results are discussed in the light of geophysical observations made at the scale of the Earth on the slip dynamics in active faults.

Introduction. – As initially proposed by Amontons in 1699 [1], the resistance to slip of an interface can be modelled by two main frictional states: static friction, that describes the strength of an interface between two solids with no relative motion, and sliding friction, that describes the contact force when the two solids slide past each other. Considering elastic deformable solids in contact, the transition from the static state to the sliding state does not happen as an instantaneous block process. Instead, there is a dynamic to consider to describe how and where the slip initiates and how it propagates along the whole interface to eventually lead to a global sliding.

Only recently did friction experiments allow following the dynamics of interface failure. Pioneer measurements, using punctual acoustic records, found that the rupture of the interface nucleates on a well-defined location, and then accelerates until reaching a velocity close to the shear wave speed of the solid [2,3]. However, imaging of the rupture at the interface was not possible. More recently, Rosakis *et al.* [4] developed a laboratory experiment where a photo-elastic solid containing a pre-defined interface was squeezed in a biaxial apparatus and rupture propagation was imaged using a high speed camera. It was shown that supershear ruptures (*i.e.* propagating at a velocity greater than the shear wave speed of the material) could propagate and the shock waves of such ruptures could be identified. This idea was pursued by Nielsen *et al.* [5,6] who built a biaxial rig where rupture nucleation was delicately controlled and its propagation was followed by photo-elasticity. In these experiments, the models are bi-dimensional and the wave field is monitored along a plane perpendicular to the sliding interface. Baumberger *et al.* [7] studied the friction of a gelatin block over a glass surface, following the friction dynamics by filming the interface through the glass. There, pulses of slip fronts could be followed directly along the plane containing the interface. Rubinstein *et al.* [8] designed an experimental set-up of friction between two transparent glass polymers, measuring optically the actual contact surfaces area and how it varies during a variety of slip events, whose velocity was ranging from ultra-slow (*i.e.* far below material wave speed) to supershear speed [9]. In all these experiments, the wave field of several ruptures could be imaged in 2D. An experimental method to capture ruptures in 3D, with a high time resolution, remains to be developed.

Here, we report on a friction experiment coupled to ultrafast ultrasonic speckle interferometry, a novel acoustic imaging technique initially developed for medical purposes in the field of elastography [10]. This technique is well-resolved in space and time and gives access to the full shear wave field radiated within the bulk in two planes of interest. It is used successfully to follow the dynamics of friction along a sliding interface. After presenting the

(a) E-mail: soumaya.latour@ujf-grenoble.fr
(b) Present address.

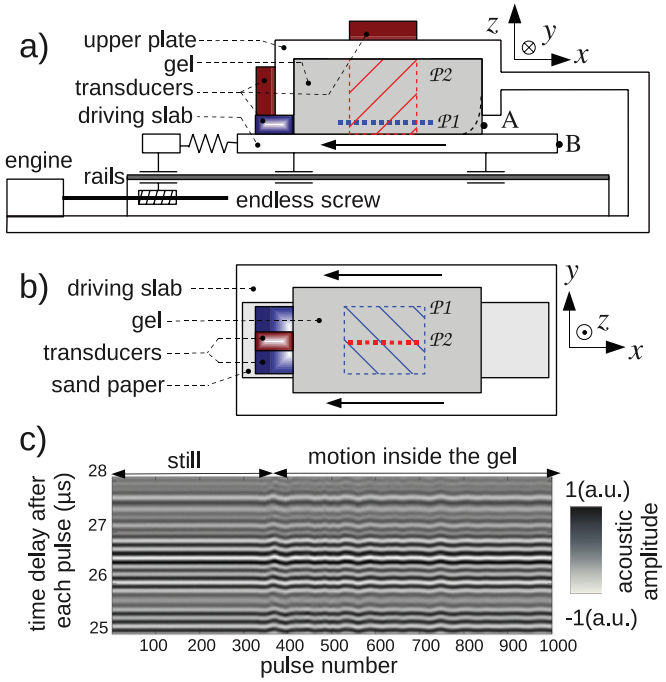

Fig. 1: (Colour on-line) Side view (a) and top view (b) of the experimental setup (see explanations in text); (c) represents 1000 acquisitions after emission of acoustic pulses on one transducer.

principle of the imaging technique, two slipping regimes are characterised.

Ultrasonic speckle interferometry in soft materials. – The friction experiment we developed couples classical macroscopic measurements (force, displacement) to ultrafast acoustic imaging at the mesoscale level of the frictional interface and of the bulk.

The home-built experimental apparatus is detailed in fig. 1. The gel slider is held by the upper plate. The ultrasonic transducers array used for speckle interferometry is fixed to the upper plate and therefore is immobile relatively to the slider. The driving slab moves under the gel on low-friction rails. The traction imposed on the driving slab during motion is measured by a force sensor (spring in fig. 1). This sensor is fixed to the plate and to a intermediate piece pulled by a motor via an endless screw. This piece also slides on the low-friction rails. Optical displacement sensors (not represented here) measure the positions of point A (deformation of the gel at the edge) and point B (driving velocity). The ultrasonic transducers array can be set on several positions allowing to image either the horizontal plane $\mathcal{P}1$, located 8 mm over the interface (position of transducers represented in blue) or the vertical plane $\mathcal{P}2$, that contains the interface (two positions of transducers represented in red). The slider is submitted to normal stress due to the weight of the upper plate. It is also sheared by the horizontal motion of the driving slab (along $-\hat{x}$). The slider is first deformed and finally reaches a frictional state in which the global frictional force varies around a constant mean value. Observations are made in this regime.

The $18 \times 6 \times 6\,\mathrm{cm}^3$ hydrogel sliders are constituted of a tangle of PolyVynilAlcool (PVA) polymeric chains holding up to 95% of water [11]. Cellulose particles are added during its confection to play a role of acoustic scatterers. This hydrogel is elastic over a large range of deformation or stress. It is a very soft solid, that can be easily sheared but is quite incompressible. This results in a high propagation speed for the compressional waves and a low propagation speed for the shear waves. In the gel, we measured by transient elastography [12] the shear wave speed $c_S = 4.1 \pm 0.2\,\mathrm{m/s}$ while the sound wave speed $c_P \simeq 1500\,\mathrm{m/s}$ is like in water.

This large difference between c_S and c_P allows using compressional ultrasonic waves to image the propagation of shear waves in the hydrogel: this is the principle of ultrasonic speckle interferometry, a method originally developed for medical imaging that takes advantage of the softness of human tissues[10]. In this technique, classical sonograms are produced by sending an ultrasonic pulse and recording all the echoes coming back from the scatterers. Each scatterer can be localised by a simple time of flight rule since c_P is homogeneous in the hydrogel. If the cellulose scatterers move under the effect of shear waves between two ultrasonic pulses, their positions on the sonogram change. Therefore the displacement of each scatterer will be recorded through time [13]. The ultrasonic array, a line of 64 ultrasonic emitters-receivers distributed on 4.8 cm, emits ultrasonic pulses at a rate of 2000 Hz. The pulses have a central frequency of 6 MHz, and are emitted simultaneously by the 64 transducers. This creates planar waves that propagate in the plane in front of the probe. The emitted plane waves are back-scattered by the cellulose acoustic scatterers and recorded by the transducers after each emission (sampling frequency is 40 MHz).

The principle of ultrasonic speckle interferometry is as follows. The transducers being highly directional, the signal received by a transducer at a time t after the emission of one pulse has been diffracted by a scatterer located in the ultrasonic beam at a distance of $c_P t/2$ (corresponding to a forth-and-back path in a duration t). The phase and amplitude of the signal in a short time window around t are determined by the distribution of the scatterers around this location in the gel. Subsequently, if the gel has not moved, the signal received after two successive emissions is exactly the same. However, if some motion inside the gel results in an increasing or decreasing distance between the transducers and these scatterers, then the echoes are received slightly later or earlier. In fig. 1(c), the records of one transducer during 1000 ultrasonic pulses at 2000 Hz is represented. It can be seen that the gel in the beam is still until the 360th pulse and is submitted to some motion after that. The displacement of the gel between two successive emitted pulses can thus be retrieved. Knowing the duration between two pulses, this gives an approximation of the instantaneous particle

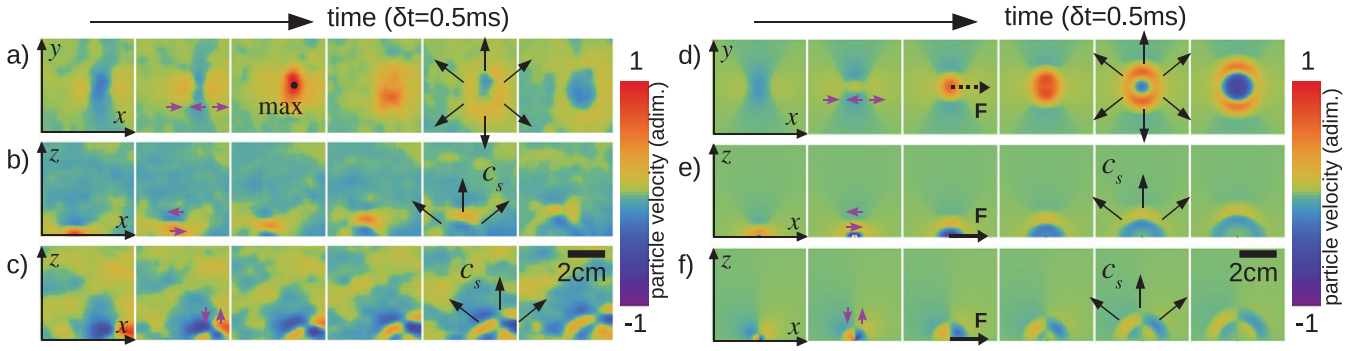

Fig. 2: (Colour on-line) Left part: experimental observations of events occurring during friction between the gel and the sandpaper. (a) Observation along the plane $\mathcal{P}1$ of the component v_x. (b) Observation along the plane $\mathcal{P}2$ of the component v_x. (c) Observation along the plane $\mathcal{P}2$ of the component v_z. The images areas are $4.5 \times 4.5\,\mathrm{cm}^2$ and the time-step is 0.5 ms between each frame. The amplitudes are normalised to get a maximum of 1 on each line. Many similar events are observed, with variable amplitudes but same radiative pattern. Right part: Green function computation gives the theoretical response of the gel submitted to a horizontal punctual and temporally Gaussian force applied at the interface 0.5 ms before first frames in the **x**-direction (represented by $\boldsymbol{F}$ in third frames). (d) plane $\mathcal{P}1$, v_x; (e) plane $\mathcal{P}2$, v_x; (f) plane $\mathcal{P}2$, v_z. The purple arrows materialise the direction of the imaged component in each case.

velocity, or to be more specific, its component along the acoustic emission direction. The signal is truncated in time windows for the 64 transducer and processed to finally give the particle velocity in the plane in front of the transducers, at each time step of 0.5 ms.

Hence, the Eulerian field of one-component particle velocity is reconstructed with a precision of 2 mm/s in the plane in front of the probe, at a rate of 2000 Hz and with a spatial resolution of the millimetre order. The shear wave speed being around 4 m/s, this is largely sufficient to follow shear waves fronts propagation in the gel. Moreover, it permits to observe all the friction phenomena that occur at the interface with velocities of the same order or lower than c_S, typically during dynamic rupture propagation.

In the following we apply this experimental method to image two kinds of frictional processes: i) friction of the hydrogel on bare sandpaper, ii) friction of the hydrogel on glass with an intermediate monolayer of sand. We demonstrate that changing the nature of the frictional interface (rough *vs.* granular) results in two different regimes of dynamic friction and discuss these regimes in light of recent observations made in geophysics on the variety of slip patterns along active faults.

Friction on sandpaper: slow slip with depinning events. – In this experiment, we glue a sheet of coarse-grained sandpaper on the driving slab. The sandpaper stripe is slightly narrower than the gel slider (see fig. 1(b)). The driving velocity is -2.7 mm/s. During the frictional motion of the gel, we observe by ultrasonic speckle interferometry multiple punctual events localised onto the interface. The typical temporal evolution of the events is represented in fig. 2, with three different configurations of the acoustic sensor that permit to get information in the planes $\mathcal{P}1$ and $\mathcal{P}2$, with access to two components of the particle velocity in plane $\mathcal{P}2$. These observations are not simultaneous as they necessitate different configurations of the transducers array (only one component in one plane can be recorded at a time). The events can be decomposed into two phases. A first phase is characterised by a static radiation pattern (snapshots between 0 and 1 ms in fig. 2). It is followed by a propagative phase that starts with a peak of particle velocity localised on the interface (at 1 ms), and then the propagation of a shear wave in the bulk (1.5 ms and later on).

To explain the source of these events, we observed, after the experiment, that the frictional surface of the gel has become rougher and that some small pieces of matter have been pulled out of the gel by the sand paper and have formed rolls of millimetre size. It is probable that during friction, some locations of the gel pin on the sandpaper and are then slowly stretched due to the motion of the driving slab. When these links fail, either because the gel depins off the sandpaper or because a piece of gel breaks, a sudden impulsive elastic shear force in the direction opposite to the driving velocity is released at the gel interface. To confirm this analysis, we calculated the full 3D elastic response of an elastic body where a shear force is suddenly applied, using the analytical elastic solution (see, *e.g.*, Aki and Richards [14]). In fig. 2(d)–(f), we display the velocity into the gel due to a horizontal force directed in the $\hat{x}$ -direction (neglecting the finite boundary conditions), characterised by the following elastic Green function. It describes the j-th component of the displacement produced by a Dirac force applied at $\vec{r}=0$ and $t=0$ in the direction $\hat{x_i}$:

$$G_{ij}(\vec{r},t) = \frac{1}{4\pi}\left[\frac{1}{c_P^2 r}\frac{x_i x_j}{r^2}\delta\left(t-\frac{r}{c_P}\right) + \frac{1}{c_S^2 r}\left(\delta_{ij}-\frac{x_i x_j}{r^2}{}_i\right)\delta\left(t-\frac{r}{c_S}\right) + \frac{1}{r^3}\left(\frac{3x_i x_j}{r^2}-\delta_{ij}\right) t\Pi_{r/c_P}^{r/c_S}(t)\right].$$

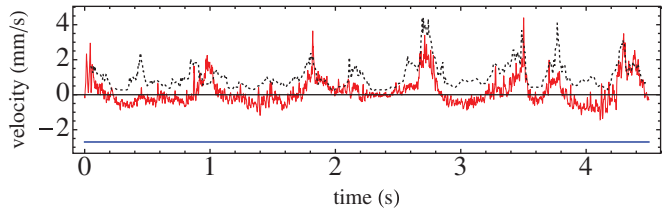

Fig. 3: (Colour on-line) Red continuous curve is the global velocity of the observed part of the gel. The blue horizontal line is the driving velocity of the slab. The dotted curve represents the depinning activity (with arbitrary units, see explanations in text). The variations of the depinning activity is correlated with the slip velocity (coefficient of correlation equals 0.67).

In this elastic response, the first two terms correspond to the compression wave and the shear wave, respectively. The third term contains near-field contributions. In our case, this last term mostly explains the radiative features observed before the S-wave propagation (two first frames in fig. 2(a), (d)). The near-field contribution is significant between the arrival time of the compressional waves and the arrival time of the shear waves, as expressed by the boxcar function $\Pi_{r/c_P}^{r/c_S}$. Due to the high difference between c_S and c_P, this time is longer in the gel than what is usually observed in more classical elastic solids (rocks, metals). The compressional waves go through the gel almost instantaneously with respect to the observation sampling rate, and the near-field contribution is observed before the arrival of the shear waves. One can note that the near-field contribution can be highly non-intuitive. For example in the first two frames of fig. 2(d), the first motion observed in response to a force $\boldsymbol{F}$ in the $\hat{x}$ direction is along $-\hat{x}$ (blue areas on these frames). The good concordance between the theoretical elastic field and the observations confirms the occurrence of depinning events at the interface radiating these characteristic patterns.

To characterise the behaviour of the gel at a larger scale of space and time, we recorded sliding during 4.5 s, imaging the x-component of the particle velocity on a $4.5 \times 5\,\mathrm{cm}^2$ area of the plane $\mathcal{P}1$, parallel to the interface. The mean value of the particle velocity on the entire plane at each time step gives the global velocity of the gel as a function of time (red curve in fig. 3). A low-frequency signal, with a periodicity close to one second, emerges in this curve. This periodicity can be related to a process of successive coupling and decoupling of the interface. The partial coupling permits some loading phases (gel velocity negative) followed by unloading phases (gel velocity positive). The unloading phases last 0.2 to 0.4 s and are related to a slow slip of the gel with respect to the sandpaper.

In the same time window, we measured all the depinning events and their locations on the $4.5 \times 5\,\mathrm{cm}^2$ surface area. A total of 660 events could be detected. An amplitude was attributed to each of them by measuring the peak value of the particle velocity (value at black point in fig. 2(a)) and subtracting the average velocity at the time of the event. We detected amplitudes going from 8.3×10^{-4} m/s to 6.5×10^{-2} m/s. Examination of the locations of the events in space and time show that some zones of the interface are more active than others but there is no evidence of a migration in relation with slow slip. We then studied the global temporal behaviour of depinning. The black curve in fig. 3 is the emission rate due to depinning, smoothed with a 30 ms time window. The peaks of this curve corresponds to periods of more frequent occurrences of large depinning events.

Figure 3 shows that these intensive depinning periods correlate with the phases of slow slip of the gel. Qualitatively, this observation is comparable to the statistical description of friction developed in [15], that links the slip periods of stick-slip friction to a massive failure of elastic contacts. Furthermore, even though there is a correlation between the velocity of the gel and the depinning activity, one can note that this correlation is not complete. Almost every phase of slow-slip (peaks of red curve) occurs together with a depinning crisis (peaks of black curve), but the amplitude of the depinning crisis is not directly linked to the amplitude of the velocity. Moreover, some depinning crisis occur without any significant peak of velocity being observed simultaneously (*e.g.* at 0.5 s or 2.2 s). At the scale of the Earth, slow slip events have been observed in some subduction zones. They are defined by large time scale (weeks to months) relaxation of tectonic loading, instead of brutal seismic release (seconds). It has been observed in Cascadia area (USA) that the slow slip occurred simultaneously with tremors crisis [16]. Tremors are low seismic signals whose source mechanisms are not well identified for now. These mechanisms are obviously different from the depinning events in the hydrogel friction, but in both cases a phenomenon at a large spatio-temporal scale (slow-slip) occurs together with a radiative activity at a smaller spatio-temporal scale (tremors in the Earth, depinning events in this experiment). The equivocal correlation between the two phenomena has also been observed in the Earth: tremors crisis can occur without any simultaneous observation of a slow-slip event or the amplitude of the slow-slip is not linearly linked to the intensity of the tremor crisis [17].

Friction along a granular interface: supershear propagation of ruptures. – In a second type of experiments, we study the effect of the presence of non-cohesive grains along the interface. For this, the hydrogel block is put on calibrated sand then removed, such that capillary forces allow adhesion of sand grains on its surface. The gel such prepared is put on a glass plate glued on the driving slab. During the friction, the sand sticks to the gel and the friction occurs between the sand layer and the glass. After a shear loading phase, a classical stick-slip behaviour sets on. A global friction coefficient was measured to be 0.6 ± 0.1, a smaller value that in the previous experiments in which it was measured 0.8 ± 0.1. During the stick-slip, we image shear waves propagating inside the gel.

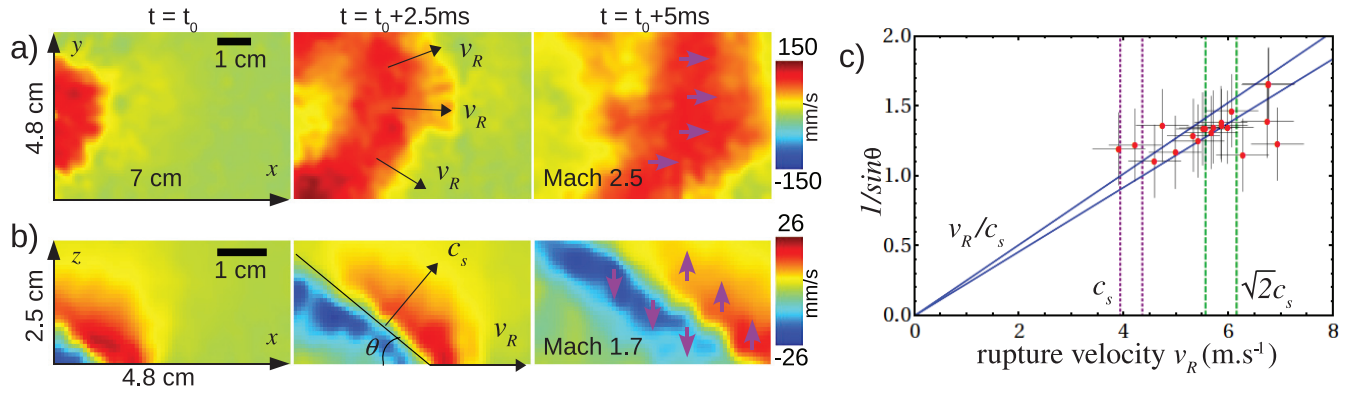

Fig. 4: (Colour on-line) (a) Observation of a supershear slipping front in the horizontal plane $\mathcal{P}1$ parallel to the interface. The colour scale is the v_x component of the particle velocity as materialised by purple arrows in the third frame. The rupture propagates roughly in the $\hat{x}$-direction, at velocity 2.5 times higher than c_S. (b) Observation in the vertical plane $\mathcal{P}2$ of a Mach front send by a supershear rupture propagating at the interface (bottom line of frames). The colour scale represents the v_z component of particle velocity (see purple arrow in the third frame). The rupture velocity for this event is 1.7 times higher than c_S (note the different spatial scales between (a) and (b)). Original AVI files (2.7M) are provided in electronic material (`movieVxPlaneP1.avi`, `movieVzPlaneP2.avi`). (c) Verification of the Mach relationship between θ and v_R using results of two 7.5 s long experiments. The blue lines have slopes $1/c_S$ and correspond to the theoretical relationship, the purple vertical lines materialise the value of c_S and the green ones $\sqrt{2}c_S$. In each case the two lines correspond to the extreme values of c_S due to the uncertainty $c_S = 4.1 \pm 0.2$ m/s.

Imaging the plane $\mathcal{P}1$, parallel to the interface, shows that slipping fronts (fig. 4(a)) move along the interface in the direction of the free edge (left side in fig. 1). The slipping fronts are variable in amplitude, shape and velocity. However, some stable features can be noticed. First of all, the slip always initiates at the locked side of the gel, and propagates towards the free edge. Only some of the ruptures cross over the whole interface, the other ones stopping before reaching the free edge. These slipping fronts are observed for tested driving velocities in the range 1 mm/s to 9 mm/s. At higher driving velocities, the slipping fronts occur more frequently. However, when the driving velocity is too large, it becomes difficult to distinguish separate events. We thus carried the majority of our further observations at the driving velocity of 1 mm/s.

The second interesting characteristic of these fronts is their velocities of propagation. We measured the velocity of propagation for each observed rupture and found values ranging from 4 m/s to 14 m/s with an estimated error of ± 0.5 m/s. These values must be compared to the shear waves speed measured in the gel, $c_S = 4.1 \pm 0.2$ m/s, which shows that the rupture fronts are propagating at supershear velocities. The slipping fronts thus should emit shear waves in the bulk as planar Mach wave fronts. This is confirmed by the observations in the vertical plane $\mathcal{P}2$ (see fig. 4(b)). The Mach front appears clearly, forming an angle θ with the interface (bottom line of the image). The slipping front propagates on this interface and drags the Mach wave behind. The angle θ is related to the rupture velocity v_R and the shear wave speed c_S through the geometrical relationship:

$$\sin\theta = \frac{c_S}{v_R}. \qquad (1)$$

To confirm this observation, we performed two 7.5-seconds experiments, and measured v_R and θ for all the ruptures that cross the observation zone. The results are summarized in fig. 4(c) where the geometrical relationship is verified through the plot of $1/\sin\theta$ *vs.* v_R. Taking into account the measurements uncertainty, the geometrical relationship is verified. We removed from this graph one data point, for which the measured rupture velocity was 14.1 ± 0.5 m/s, but $1/\sin\theta = 2.0 \pm 0.3$. This point, clearly out of the theoretical curve, can probably be explained by an unusual direction of propagation for the rupture front, forming a large angle with the x-axis, and resulting in the measurement of an apparent rupture velocity in the plane of observation $\mathcal{P}2$. This bias is of course present in all the data of this graph, but can normally be considered small given that the majority of the rupture fronts propagate in a direction globally parallel to the x-axis.

The repartition of the velocities of the ruptures presents an accumulation around $\sqrt{2}c_S$ (fig. 4(c)). This is the theoretical value over which supershear ruptures are expected to be stable [18]. However, ruptures with much higher velocity were also observed, for example 10 ± 0.5 m/s in the event of fig. 4(a). Fast supershear ruptures have already been observed in few laboratory experiments [4,19,20]. Until now, we could not show any obvious relationship between the amplitude of the events and their velocity. Systematic studies will be necessary in the future to characterise statistically these rupture fronts and show if a clear trend may emerge.

Supershear ruptures have been observed in several earthquakes on tectonic faults. The first observation was performed during the 1979 Imperial Valley earthquake [21]. It was later observed over longer distances during the 1999 Izmit earthquake [22], the 2001 Kunlun

earthquake [23] and the 2002 Denali earthquake [24]. Seismologists interest in such rupture modes is due to the Mach front, which can create co-seismic ground accelerations higher than what is produced by usual subshear ruptures. This may increase seismic hazard significantly. It is generally accepted that the heterogeneity of the fault frictional properties and/or of the initial stress level play an important role in the appearance of supershear earthquake [25]. The previously cited examples of supershear earthquakes all occurred in long and very linear faults [26], suggesting that they can be characterised by a low level of heterogeneity. In the present experiments, this criterion is fulfilled since the frictional property of the interface is defined by the friction of the sand on the glass, and the sand layer is quite homogeneous. This homogeneity of the friction properties may result in a small difference between the static stress threshold and the shear stress at the interface when the rupture begins, thus favoring supershear rupture propagation [27]. It can be noted that this sliding regime is highly different from the case of friction of gel on sandpaper. In the case of the sand paper, the surface is sliding almost freely except for the random pinning of some points of the gel. The pinned points act like barriers that prevent the outbreak of a slip instability [25], leading to slow slip and the absence of rupture propagation.

Conclusion. – We built an original friction experiment that allows the study of dynamic friction. The ultrafast ultrasonic speckle interferometry technique, taking advantage on the difference of the propagation speeds of the compressive and shear waves in soft solids, permits to record the Eulerian field of one-component particle velocity in two planes of interest. We report the first experiments, in which we identified and characterised two slipping regimes. This experiment showed its capacity to study dynamic friction, a problem of high interest in many fields of physics, and particularly in seismology. From this point of view, it is interesting to note that the two slipping regimes we obtain are observed in seismic faults. Yet, until now, we did not produce any dynamic subshear rupture, which are supposed to be the most current type of earthquake ruptures. In future work, we shall study the effects of heterogeneity on the slipping regime and take advantage of the spatial accuracy of this method to obtain experimental observations of the interaction of a slipping front with a localised heterogeneity, a problem widely studied numerically, but almost not documented in an experimental point of view. Finally, we have built an efficient tool to study rupture dynamics, which will be used in the future to investigate current issues in earthquake source dynamics.

* * *

The experimental apparatus was constructed with the technical support of B. Vial and A. Richard and funded by the ANR project JCJC-0011-01.

REFERENCES

[1] Amontons G., *Mem. Acad. R. Sci.* (1699) 206.
[2] Okubo P. and Dieterich J., *J. Geophys. Res.*, **89** (1984) 5817.
[3] Ohnaka M., Kuwahana K., Yamamoto K. and Hirasawa T., in *Earthquake Source Mehanics, AGU Geophys. Monogr.*, edited by Das S., Boatwright J. and Scholz C., Vol. **37** (American Geophysical Union, Washington) 1986, p. 13.
[4] Rosakis A., Samudrala O. and Coker D., *Science*, **284** (1999) 1337.
[5] Nielsen S., Taddeucci J. and Vinciguerra S., *Geophys. J. Int.*, **180** (2010) 697.
[6] Schubnel A., Nielsen S., Taddeucci J., Vinciguerra S. and Rao S., *Earth Planet. Sci. Lett.*, **308** (2011) 424432.
[7] Baumberger T., Caroli C. and Ronsin O., *Eur. Phys. J. E*, **11** (2003) 85.
[8] Rubinstein S. M., Cohen G. and Fineberg J., *Phys. Rev. Lett.*, **98** (2007) 226103.
[9] Ben-David O., Cohen G. and Fineberg J., *Science*, **330** (2010) 211.
[10] Sandrin L., Catheline S., Tanter M., Hennequin X. and Fink M., *Ultrason. Imaging*, **13** (1999) 111.
[11] Fromageau J., Genisson J.-L., Schmitt C. L. M. R., Mongrain R. and Cloutier G., *IEEE Ultrason. Ferroelectr. Frequency Control.*, **54** (2007) 498.
[12] Catheline S., Wu F. and Fink M., *J. Acoust. Soc. Am.*, **105** (1999) 2941.
[13] Gallot T., Catheline S., Roux P., Brum J., Bench N. and Negreira C., *IEEE Ultrason. Ferroelectr. Frequency Control.*, **58** (2011) 1122.
[14] Aki K. and Richards P., *Quantitative Seismology* (University Science Books) 2002.
[15] Braun O. and Peyrard M., *Phys. Rev. Lett.*, **100** (2008) 036117.
[16] Rogers G. and Dragert H., *Science*, **300** (2003) 1942.
[17] Kostoglodov V., Husker A., Shapiro N. M., Payero J. S., Campillo M., Cotte N. and Clayton R., *Geophys. Res. Lett.*, **37** (2010) L24301.
[18] Burridge R., Conn G. and Freund L., *J. Geophys. Res.*, **84** (1979) 2210.
[19] Xia K., Rosakis A. and Kanamori H., *Science*, **303** (2004) 1859.
[20] Rubinstein S. M., Cohen G. and Fineberg J., *Nature*, **430** (2004) 1005.
[21] Archuleta R., *J. Geophys. Res.*, **89** (1984) 4559.
[22] Bouchon M., Toksoz N., Karabulut H., Bouin M., Dietrich M., Aktar M. and Edie M., *Geophys. Res. Lett.*, **27** (2000) 3013.
[23] Bouchon M. and Vallee M., *Science*, **301** (2003) 824.
[24] Dunham E. and Archuleta R., *Bull. Seismol. Soc. Am.*, **94** (2004) S256.
[25] Latour S., Campillo M., Voisin C., Ionescu I. R., Schmedes J. and Lavallée D., *J. Geophys. Res.*, **116** (2011).
[26] Bouchon M., Karabulut H., Bouin M.-P., Schmittbuhl J., Vallée M., Archuleta R., Das S., Renard F. and Marsan D., *Tectonophysics*, **493** (2010) 244.
[27] Andrews D., *J. Geophys. Res.*, **81** (1976) 5679.